International Journal of Electronics and Applied Research (IJEAR) **vol. 4, issue 2, Dec 2017**
Online (*http://eses.net.in/ESES Journal)* ISSN 2395-0064

Note on discussion about the possible troposphere tide influence on the longitudinal distribution of the equatorial plasma bubbles

L.N. Sidorova and S.V. Filippov
Pushkov Institute of Terrestrial Magnetism, Ionosphere and Radiowave Propagation (IZMIRAN), Kaluzhskoe shosse, d.4, 108840 Moscow, Troitsk, Russia

Abstract

In this paper we consider an idea of the troposphere tide influence on the character of the longitudinal variations in the distribution of the equatorial plasma bubbles (EPBs) observed in the topside ionosphere. For this purpose, the obtained longitudinal EPB patterns were compared with the thermosphere characteristics having the prominent "wave-like" longitudinal structures with wave number 4, which are uniquely associated with the influence of the troposphere DE3 tides. The characteristics of the equatorial mass density anomaly (EMA) and zonal delta wind were used for comparison. The equinox seasons during high solar activity were under consideration. It was obtained that the longitudinal patterns of the EMA and zonal delta wind show the surprising similarity with the EPB distributions ($R \cong 0.8$, $R \cong 0.72$). The obtained numerical estimations show that the thermosphere zonal winds are the most possible transfer mediator of the troposphere DE3 tide influence. The most successful moment for the transfer of the troposphere DE3 tide energy takes place in the beginning of the EPB production, namely, during the seed perturbation development.

Key Words: *1. topside ionosphere; 2. equatorial plasma bubbles; 3. troposphere tide influence*

1. Introduction

The longitudinal distributions of the equatorial plasma bubbles (EPBs) are extensively investigated during the last decades. These distributions were explored for the different helio- and geophysical conditions and different altitude ranges. The observation altitudes vary from the altitudes above the *F* peak, where the initial plasma depletions invert into the plasma bubbles, up to the topside ionosphere. The EPBs obtained above the *F* peak were studied by [McClure et al., 1998; Basu et al., 1976] based on the AE-E (~300–475

km) and OGO-6 (~400–500 km) satellite data, respectively. The EPBs detected at the topside ionosphere altitudes have been studied more extensively and presented in the publications of [Watanabe and Oya, 1986] (Hinotori satellite data, ~650 km), [Su et al., 2006; Li et al., 2007, 2008] (ROCSAT-1 satellite, ~600 km) and [Li et al., 2007, 2008] (DMSP F15 satellite data, ~840 km). Moreover, there are the investigations of the EPBs [Maruyama and Matuura, 1980, 1984; Sidorova and Filippov, 2012] seen at the altitudes greater than 1000 km (ISS-b satellite data, ~972–1220 km). The plasma bubbles, reaching their "ceiling" altitudes in the topside ionosphere, often called as "dead bubbles" [Aggson et al., 1992] or fossil bubble signatures [Sidorova, 2007]. They are hardly detected in *Ne* density but they become "visible" in the minor species (e.g., in He^+ density) since the background He^+ density strongly increases at the upper topside altitudes and shows contrast with insignificant small He^+ density content inside the plasma bubble [Sidorova, 2004, 2007, 2008; Sidorova and Filippov, 2012, 2014]. These plasma bubbles detected at the upper topside altitudes are of special interest of this study.

According to [McClure et al., 1998; Su et al., 2006; Li et al., 2007, 2008; Sidorova and Filippov, 2012] the longitudinal EPB distributions show the prominent variability from season to season, from hemisphere to hemisphere. For example, the longitudinal EPB distributions taken in the different hemispheres in the same season are essentially different. There is difference in the values of their occurrence probability maxima; there is some longitudinal shift between these peaks [Sidorova and Filippov, 2012]. Doubtless a specific influence of the geomagnetic field plays the fundamental role in the longitudinal shifts of the global probability maxima. The plasma bubbles (as charged depleted areas) are controlled by the geomagnetic field during their uplift and "stretching". The difference in the magnetic field declination significantly showing in the different hemispheres leads to these shifts. This reason is considered as main one determining the character of the longitudinal variations of the topside ionosphere.

The seasonal factor is responsible for amplitude variability of the longitudinal probability maxima. We imply that the seasonal factor shows itself not only in the insolation difference of the different hemispheres but also in the seasonal wind variability. Seasonally modulated neutral zonal winds in combination with the geomagnetic field declination can enhance (reduce) the vertical field-aligned winds resulting in regions of larger (smaller) plasma density [Watanabe and Oyama, 1996]. Moreover, such modulated vertical field-aligned winds can also promote ("lock") the equatorial spread-F and EPB development [Abdu, 2001].

As a whole, variability of the longitudinal EPB occurrence rate is well enough explained by the mentioned above reasons. However, still some questions arise. There are the cases when the EPB statistical plots demonstrate the distinctly pronounced 4 maxima. Such prominent "wave-like" structures with wave number 4 are especially well seen during the equinox periods [Li et al., 2007, 2008; Sidorova and Filippov, 2012]. It is reasonable to ask about the reasons and sources of these longitudinal four-cell patterns.

It is worthy to mention that the numerous messages about the similar four-peak longitudinal structures have appeared in the recent years. These structures are distinctly observed in the maps of the thermosphere neutral winds [Häusler et al., 2007; Yizengaw, 2012] and equatorial mass density anomaly (EMA) [Liu et al., 2009]. The four-peak wave structures are confidently determined in the ionosphere, namely, in *F* region plasma and electron density [Lühr et al., 2007; Jin et al., 2008; Fang et al., 2009], in total electron content (TEC) of the *F* region and topside ionosphere/plasmasphere [Pedatella et al., 2011].

The DE3 oscillations can affect the thermosphere parameters (temperature, mass density) and ionosphere parameters (*Ne* and *Ni* density) through the modulation of the thermosphere winds and electric fields. Namely, the DE3 oscillations can modify the wind-driven *E* region dynamo. The last one, in turn, modifies the ionosphere **E×B** drift and fountain process [Immel et al., 2006; Jin et al., 2008], which are responsible for lifting the equatorial plasma and formation of the equatorial ionosphere trough. The result of this modulating effect is the formation of a four-peak longitudinal structure, e.g., in the equatorial ionization anomaly (EIA) distribution [Fang et al., 2009].

Note that the mentioned coupling scheme is fair during daytime only, when the *E*-layer dynamo dominates. There are some peculiarities in the post-sunset period. The post-sunset four-peak wave structures of the EIA exhibits larger amplitude than that during daytime [Liu and Watanabe, 2008]. Hence, they can hardly be interpreted as a remnant structures formed during daytime. [Liu and Watanabe, 2008] suggest that the four-peak structure is intensified, possible, by the pre-reversal **E×B** drift enhancement (PRE).

Meanwhile, it is well known that the equatorial plasma bubbles generated in the post-sunset periods are controlled by the PRE. Due to the PRE the equatorial plasma and the separate irregularities (including the plasma bubbles) start to uplift to the topside ionosphere altitudes.

At the first glance, it is reasonable to suppose that the PRE is a possible energy transfer mediator of the thermosphere tide influence, which can induce the four-cell patterns in the longitudinal plasma bubble

distribution. Namely, the DE3 tides can be "translated" (due to the modulation of evening equatorial **E×B** drift, PRE) to the topside ionosphere and "blurred" (due to the fountain effect) in the low-latitudinal region. As a result, the uplifting plasma bubbles controlled by the geomagnetic field and modulated **E×B** drift can show the four-cell longitudinal patterns. Some attempts to reveal this connection was made by the different groups of the investigators [Li et al., 2008; Kil et al., 2015; Sidorova and Filippov, 2016]. It was shown, however, that the four-peak longitudinal structure of the EPB occurrence rate is correlated with the longitudinal structure of evening EIA only [Henderson et al., 2005; Li et al., 2008]. This correlation is moderate ($R \cong 0.37$), meantime the correlation with PRE is negligible ($R \cong 0.12$) [Sidorova and Filippov, 2016].

Hence, there is some doubt that the mentioned transfer of the troposphere influence is the only way. Especially since there are the indications [Kil et al., 2015] that the effect of DE3 on the *F* region decreases after sunset due to the reduction of the *E* region conductivity, and therefore, the DE3 signature is a weak feature in PRE. Hence, there is a sense to check out the other possible ways and other suitable candidates of the transfer of the troposphere tide influence. Namely, it is reasonable to examine the possibility of the direct influence of the thermosphere winds modulated by the DE3 tides.

In order to investigate the above hypotheses, the comparative analysis of the thermosphere characteristics (EMA and zonal delta wind longitudinal variations) having the typical four-peak wave structures will be made. Also, the numerical estimations based on the theory of [Kudeki and Bhattacharyya, 1999] dealing with the seeding mechanism in the EPB generation will be obtained.

2. **Data**

As it was pointed, the modulations by the DE3 oscillations were observed in the different steps of the thermosphere–ionosphere coupling. For example, the four-peak longitudinal wave structures were found in the thermosphere zonal wind [Häusler et al., 2007; Häusler and Lühr, 2009] and equatorial mass density anomaly (EMA) [Liu et al., 2009]. Below you can see the detailed description of these thermosphere characteristics. We should note that all data used in this study were obtained under conditions of high solar activity. Unfortunately, the thermosphere four-peak wave structures (e.g., in temperature, mass density, zonal/meridional winds) are less pronounced during this period [Oberheide et al., 2009].

2.1. Equatorial plasma bubbles (EPBs)

The EPB longitudinal statistics was obtained by using the He^+ density depletion dataset. The dataset was based on the ISS-b spacecraft operation [RRL, 1983, 1985] during the high solar activity period (1978–1979, $F_{10.7}$~200) at the topside ionosphere altitudes (~1100 km). ISS-b spacecraft was launched into a nearly circular orbit (~972–1220 km) with an orbital period of ~107 min, and with an inclination angle of ~70°. ISS-b measurement dataset covers the 17-month interval (1978–1979) with some significant gaps. For example, no July data are available; June data are partially available. However, the data of the equinoctial periods are the most complete [RRL, 1983, 1985].

Initially, ~700 cases of the He^+ density depletions (subtroughs) were registered in ~1105 passes (the passes with observations). Investigation of their latitudinal position as function of *Kp* showed that they can be readily divided into two groups [Karpachev and Sidorova, 2003]. One group (~256 cases) was detected during the periods of magnetic disturbances (or immediately after them) in the latitude band of 45°–58° (L~2–3.5). Another group (~440 cases) appears during the prolonged magnetically quiet periods at latitudes of 20°-50° (L~1.3–2.5). It was concluded that these two groups are of a different origin [Karpachev and Sidorova, 2003; Sidorova, 2007]. Examination of the literature reveals that the He^+ density depletions (subtroughs) of the first group were usually interpreted as "plasmatails" resulting from earlier storm time depletions [Chen and Wolf, 1972]. As to the He^+ density depletions observed deeply inside the plasmasphere without any connection with disturbances, [Sidorova, 2007] proposed to consider them of equatorial origin. Such depletions were interpreted as “fossil” signatures of the EPBs seen in the He^+ density [Sidorova, 2007, 2008]. This idea was well supported by the numerical estimations [Sidorova and Filippov, 2014] and validated by the statistical studies [Sidorova, 2004, 2007, 2008; Sidorova and Filippov, 2012].

The typical He^+ density plot with the mentioned He^+ density depletions (subtroughs) is shown in Figure 1. These He^+ density depletions can be detected at the different regions of the crests of the equatorial He^+ density trough: at inside slope, at top and more frequently at outside slope. We are taking into account only the well-pronounced density depletions from two-three times to two orders of magnitude of the background plasma density [Karpachev and Sidorova, 2002, 2003]. Such depletions are characterized by density dropping within 2° to 10° latitude, and therefore, they may be referred to the medium-/large-scale

ionospheric irregularities. Only the He^+ density depletions, which appear during the prolonged magnetically quiet periods ($Kp \leq 3$) at latitudes of ±20°–50° INVLAT (L~1.3–2.5), were under consideration.

It is known that the plasma bubbles are produced at the bottom-side of the *F*-layer in the post-sunset periods, i.e. around 18–19 LT. Later, they can uplift and reach the topside ionosphere heights (~1100 km). That is why the LT interval of the EPB observations is intentionally chosen as 20–04 LT.

For one comparative purpose, the longitudinal variations of the EPB occurrence probability (*P*) were obtained for the vernal equinox season of the Northern Hemisphere (NH) only. The *P* variations calculated for each geographical longitudinal bin of 15° are shown in Figure 2(a, b).

For other purpose, the longitudinal variations of the EPB occurrence probability were obtained as pattern averaged over two hemispheres and two equinoctial periods. These *P* variations are shown in Figure 3(b, c). Each equinoctial period is presented by four-month interval centered around an equinox. (For example, the vernal equinox season is considered for the period of two months before and after the equinox day.) The standard deviations of *P* were calculated as $\Delta = (P(1\text{-}P)/N)^{1/2}$, where *N* is the pass number per bin. The typical standard deviations are shown in the Figures (2, 3) by the vertical error bars.

In all cases, we have used the most complete ISS-b datasets obtained during the periods of the equinox seasons. It is expected that they can provide the most reliable results. It is worthy to note that the equinox seasons are the most opportune for our comparison aims since the DE3 tide amplitudes are the most pronounced in these months [Häusler and Lühr, 2009].

Note that we intend to consider the longitudinal variations of the thermosphere characteristics in the geographical longitudes. Since the plasma is magnetized, plasma bubbles are field-aligned in process of their uplifting. Due to the discrepancy between the geographic and geomagnetic coordinates, it is expected that the longitudinal distributions of the plasma bubbles will show the specific features depending on the hemisphere of observation. Furthermore, the difference between their longitudinal distributions will increase with latitude increasing. Since the latitude intervals of the EPB observation (±20°–50° INVLAT) are far enough from the equator, this difference will be observed very clearly. Obviously, we can minimize this difference using the calculation of the plasma bubble statistics by averaging over the hemispheres. It seems reasonable to use this approach since we intend to do the comparison with EMA longitudinal distributions [Liu et al., 2009] obtained by the similar way.

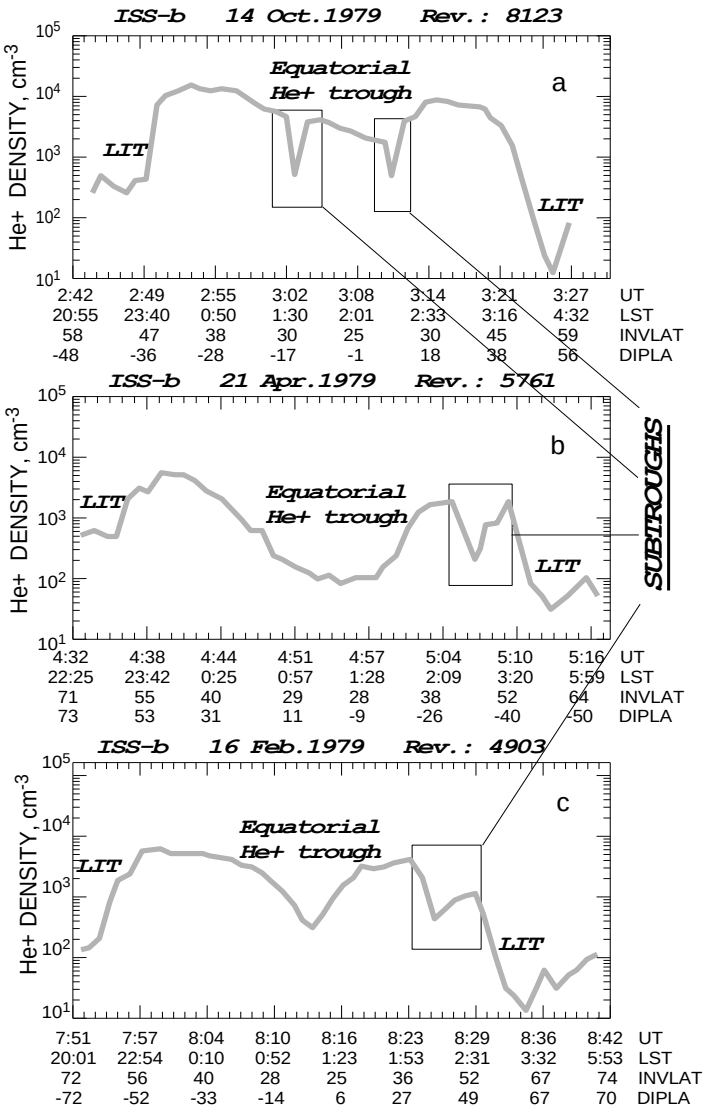

Figure 1: He^+ density depletions (subtroughs) as measured by ISS-b. (After Sidorova, 2007)

It should be noted that the thermosphere characteristics involved into comparison are given for the intervals of the geomagnetic (±10° MLAT) and dipole latitudes (±5° DIPLAT, ±20°–30° DIPLAT) (see below). Meanwhile, the plasma bubbles are observed in the intervals of ±20°–50° INVLAT (registration at the altitudes of ~1000–1200 km). It means that their low interval limit (±20° INVLAT) "captures" the latitude of the magnetic equator measured in the geomagnetic and dipole coordinates. On the other hand,

the upper limit (±50° INVLAT) overlaps (with a large margin) the intervals of the data used for comparisons. Since the mentioned intervals are completely overlapped, it is fair to compare the data.

2.2. Zonal delta wind

The four-peak longitudinal wave structures in the thermosphere zonal wind were first found by [Häusler et al., 2007]. The authors have investigated the wind deviations (zonal delta wind) from the zonal average derived from CHAMP accelerometer measurements (2002–2004, $F_{10.7}$~190–100, ~400 km). The data were taken between ±10° MLAT along the geomagnetic equator.

Two equinoctial patterns of the longitudinal variations of the zonal delta wind obtained in the pre-sunset (15–18 LT) and sunset (18–21 LT) hours [Häusler et al., 2007] were under consideration. The variations obtained by averaging over the combined period (15–21 LT) were used for the comparison (Figure 2(a)). The extended LT interval was taken intentionally to identify the steady zonal delta wind variations.

It is worthy noting that the amplitude range of the obtained variations is ±12 m/s (Figure 2(a)). Meantime, the typical mean velocities derived from the CHAMP observations taken under the same conditions are 100–200 m/s (e.g., [Liu et al., 2006]). (Positive velocity means eastward.) Hence, the mentioned variations (±12 m/s) should be considered only as perturbations of the strong background eastward zonal wind.

2.3. Equatorial mass density anomaly (EMA)

Equatorial mass density anomaly (EMA), i.e. anomaly in the total air mass density, was first observed and described by [Liu et al., 2005]. It was shown that the EMA is an anomalous latitudinal distribution of the atmospheric mass density with a density trough near the Earth's dip equator and density crests near ±25° dip latitude. In fact the EMA structure is the neutral counterpart of the well known equatorial ionization anomaly (EIA) in the ionosphere [Liu et al., 2009]. Although it is assumed that the latitude structure of the EMA is principally caused by the EIA via ion drag [Liu et al., 2005].

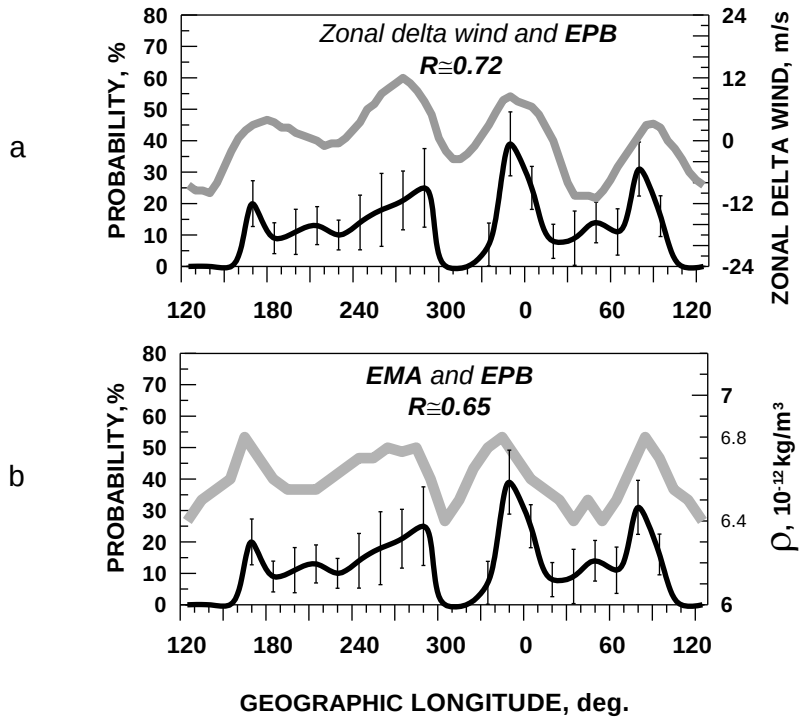

Figure 2: Longitudinal EPB distribution (*P*) obtained in NH for the vernal equinox season is shown in (a, b) by smoothing dark curve. (a) Longitudinal zonal delta wind variations obtained from [Häusler et al., 2007] for the equinoxes are shown by grey curve. Correlation factor is $R \cong 0.72$. (b) Longitudinal EMA distribution obtained from [Liu et al., 2009] in NH for the vernal equinox period is shown by light-grey curve. Correlation factor is $R \cong 0.65$.

Global distribution of the neutral density was presented by [Liu et al., 2009]. CHAMP observations (~420 km) during solar maximum year (2002, $F_{10.7} \cong 170–190$) have used. The map was built in geographic coordinates as average pattern for the equinoctial periods (March-April, August-September 2002). The density data under quiet conditions ($Kp \leq 3$) were used. Only the density data of the pre-sunset period (14–18 LT), while a four-peak longitudinal structure of EMA is the most pronounced, were under consideration.

For comparative purpose, using this distribution we have calculated the longitudinal variations of the mass density in the NH. The plot obtained by averaging density within 20°–30° DIPLAT for each geographical longitudinal bin of 10° is shown in Figure 2(b) by solid light-grey curve.

For other comparative purpose, we have taken the longitudinal EMA plots presented in the same paper [Liu et al., 2009] and obtained by averaging densities over two hemispheres. The neutral density plots (calculated for each geographical longitudinal bin of 5°) were obtained in the crest and trough regions

separately [Liu et al., 2009]. These plots obtained by averaging densities over two hemispheres within ±10°–20° DIPLAT and ±5° DIPLAT are shown in Figures 3(a) and 3(b), respectively.

3. Comparison

The main issues we want to discuss within this paper are the source of the typical variations in the longitudinal EPB distributions and our understanding the ways of the possible transfer of the troposphere tide influence. That is why the detailed comparison with the thermosphere characteristics was made.

3.1. EPBs and zonal delta wind

The EPB statistics obtained in the NH during the vernal equinox season was compared with the longitudinal zonal delta wind variations obtained in the pre-sunset and sunset hours (15–21 LT) during the equinoxes [Häusler et al., 2007] (Figure 3(a)).

Comparative analysis of the plots reveals their good similarity (Figure 3(a)) with unexpectedly high correlation factor (R≅0.72). Indeed, it is easy to note that at least three peaks of the both variations are the same shape and appear at the same longitudes. Note that the correlation coefficients obtained in the present paper were calculated using the STATISTICA 6.0 software package. The pointed correlations are statistically significant at p<0.05 (level of significance) and n=24 (number of independent data points).

3.2. EPBs and EMA

Comparison was done for two different cases shown in Figures 2(b) and 3(b, c). The EPB statistics obtained in the NH was compared with the EMA plot obtained in the crest region (20°–30° DIPLAT) of the NH (Figure 2(b)). Comparison shows very good similarity. Correlation factor was noticeable (R≅0.65; p<0.05 and n=24). Note that the similarity was seen even in the "thin" details, e.g., in the specific shape of the peak (~270°−300°) or in the appearance of the small peak near ~45°–50° longitude.

On the other hand, the EPB statistics averaged over both hemispheres and two equinoctial periods was compared with the EMA distributions obtained by the same way (Figure 3). The *maximal similarity* was

revealed for the EMA plot obtained near the neutral density crests (±20°–30° DIPLAT) (Figure 3(b)). The correlation factor was high, $R \cong 0.8$ (!). This correlation is statistically significant at $p<0.05$ and $n=24$. Comparison with the EMA plot obtained in the trough region (±5° DIPLAT) shows that the common similarity of the patterns is still kept but some "details" vanish (Figure 3(c)). As a result, the correlation factor becomes slightly worse ($R \cong 0.59$; $p<0.05$ and $n=24$).

So, the results of comparison made for the both cases show good enough similarity between the patterns. However, if the region of the crest is under consideration only, the correlation factor is much better for the plots averaged over both hemispheres. Perhaps, it takes place since the specific influence from the magnetic field deviations of the different hemispheres is maximally eliminated. The obtained high correlation suggests that either the both phenomena can be affected by the powerful external influence (maybe by the tide-induced thermosphere winds) or there is a causal relationship between the phenomena. It seems the first reason is more probable since there is distinct correlation between the EPB and zonal delta wind variations.

4. Discussion and numerical estimation

We proposed that the specific four-peak structure in the longitudinal EPB distributions can be influenced by solar thermal tides excited by latent heat in the troposphere. Let's accept this working hypothesis. It means we should discuss the probable energy transfer mediators of the troposphere tide influence.

The comparative analysis shows the high correlation ($R \cong 0.8$) between the longitudinal EPB and EMA distributions taken at the crests (±20°–30° DIPLAT) (Figure 3(b)). Moreover, there is noticeable correlation ($R \cong 0.65$) between them calculated in the NH only (Figure 2(b)). In other words, the phenomena of the different nature and of the different altitude regions show the remarkable similarity. Why?

It is worth noting that there is no perfect phase synchronism between the four-peak longitudinal wave structures seen in the EIA and EMA variations [Sidorova and Filippov, 2016]. Meantime, it is generally accepted that the EIA plays the important role in the EMA formation through ion drag and chemical heating. It is known that the locations and magnitudes of the EMA crests close follow those of the EIA. This contradiction was firstly revealed by [Liu et al., 2009]. They have pointed that "this difference

strongly suggests that although the latitudinal structure of the EMA is principally caused by the EIA via ion drag, its wave-4 longitudinal pattern likely arises from different source".

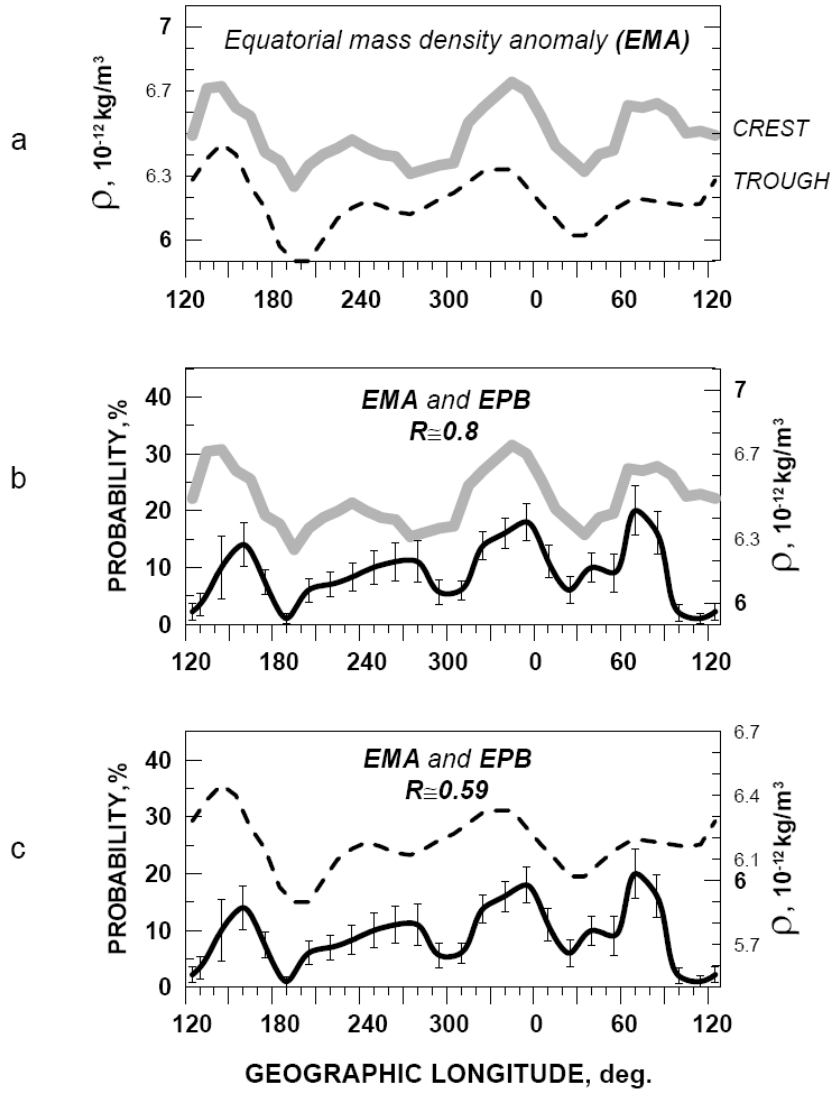

Figure 3: Longitudinal EMA distributions obtained by averaging over two hemispheres and two equinoctial periods in the crest and trough regions [Liu et al., 2009] are shown by solid grey (a, b) and dashed black (a, c) curves, respectively. Longitudinal EPB distribution obtained by averaging over two hemispheres and two equinoctial periods is shown in (b, c) by smoothing dark curve. (b) Correlation factor is $R\cong0.8$. (c) Correlation factor is $R\cong0.59$.

EMA observations [Liu et al., 2009] used for our comparison were obtained at the altitudes of ~420 km (the typical altitudes of the upper thermosphere and *F* region), whereas, as it is known, the solar tide

oscillations are generated at the troposphere altitudes (~80−100 km). According to [Liu et al., 2009] the typical wave-4 longitudinal pattern of EMA results more likely from the direct penetration of the DE3 tide to the *F* region altitudes than from EIA via ion drag. It was shown that this conclusion is consistent with the theoretical predictions and confirmed by the several observations [Oberheide et al., 2009; Oberheide et al., 2011; Forbes et al., 2009; Talaat and Lieberman, 2010].

Meantime, note that the amplitude of the longitudinal EMA variations was only ~2% even in the period (14−18 LT) of their maximal development [Liu et al., 2009]. Hence, it is reasonable to consider the EMA longitudinal effect only as possible "marker" of the direct DE3 tide penetration to the *F* region altitudes. Obviously, such weak longitudinal effect is hardly able to cause any noticeable changes in the ionosphere. In this sense, it is hard to suspect that there is a causal relationship between the EMA and plasma bubbles.

By other side, there is obvious link between the longitudinal EMA and EPB distributions, which provides their excellent correlation. That is why we should pay attention to the thermosphere winds as a most possible link and transfer mediator of the troposphere tide influence. Evidently, the both phenomena (EMA and EPBs) are affected by the powerful influence of the tide-induced thermosphere winds. (The correlation result between the EPB and zonal delta wind variations is more than convincing, R≅0.72.)

It is reasonably to discuss the possible transfer mechanism. To clarify this question, there is a sense to consider the different phases of the plasma bubble development and define the phase, when the wind influence is the most effective. Let's start with the initial phase of the EPB development.

(1) Since the pioneering study of [Woodman and La Hoz ,1976] it is widely accepted that the equatorial *F* region irregularities (EFI) (including the EPBs) are produced by the Rayleigh–Taylor (R–T) instability taking place after sunset at the bottom-side of the *F*-layer. It is believed that the R–T instability is necessary condition but not sufficient. The initial "seed" perturbations of the background plasma are the second necessary condition for the EPB generation. In other words, the occurrence probability of the equatorial *F* region irregularities (P_{EFI}) depends on the occurrence probability of the seed (P_{seed}) and R–T instability ($P_{R\text{-}T}$): $P_{EFI} = P_{R\text{-}T}P_{seed}$ [McClure et al., 1998]. However, if the development of the R–T instability is rather stable factor, the seed perturbations are the most variable from day to day, longitudes etc.

Most of the investigators believe that the acoustic gravity waves (AGWs) play an important role in the generation of the seed perturbations [Singh et al., 1997; McClure et al., 1998; Abdu, 2001; Tsunoda,

2010; Kherani et al., 2011]. Some investigators [Kudeki and Bhattacharyya, 1999; Hysell and Kudeki, 2004; Kudeki et al., 2007] believe that a collisional shear instability plays a key role in the seed perturbation appearance. In turn, the eastward thermosphere wind plays a crucial role in the development of the collisional shear instability. They claim that "plasma bubble production in any longitudinal region of the equatorial ionosphere is primary controlled by eastward neutral wind at sunset" [Kudeki et al., 2007]. Namely, the larger eastward wind produces the larger growth rate of seed perturbation, the stronger PRE and the larger uplift of the bottom-side F region. At last, there are indications [Fritts et al., 2008, Kherani et al., 2011] about the superposition effect of the AGWs and thermosphere zonal winds in the seeding mechanism.

According to [Oberheide et al., 2009; Forbes et al., 2009], DE3 tide oscillations affecting the thermosphere wind can directly penetrate to the thermosphere and ionosphere altitudes of the F region. It means that the modulation effect can be reflected in the characteristics of the plasma irregularities which occur over the equator at the bottom-side of the F-layer. Namely, the tide-induced thermosphere winds can affect the plasma bubbles (during their seeding) by the similar way like the background neutral components of the thermosphere (EMA). As a result, we can see the same longitudes, where the tide-induced thermosphere winds promote both the neutral mass density inspissation (exhaustion) and the advantage (lack) in producing the seed perturbations followed by EPBs. That is why the longitudinal EPB distribution shows the high correlation with the longitudinal EMA and zonal delta wind variations ($R \cong 0.8$ and 0.72). Concerning the seeding mechanism and possible tide influence, certainly, this conclusion is in good accordance with theory of [Kudeki and Bhattacharyya, 1999]. Their main idea is that the eastward wind-driven Pedersen currents are able to polarize F-region density perturbations (seeding perturbations) with westward tilting wavefronts into rapidly growing modes to trigger the formation of spread-F bubbles. According to [Kudeki et al.,2007] the growth rate of the seeding perturbations generated at the bottom-side of the F-layer is $\gamma \cong U/2L$ (s^{-1}), where U is the velocity of the eastward neutral wind, L is the density gradient scale length. The eastward neutral wind is determined as a key parameter for spread-F initiation during the post-sunset period. So, even the small tide-induced wind variations are able to affect the growth rate of the seeding perturbations.

Meanwhile, this conclusion is not contradictory to the results obtained by [Fritts et al., 2008] from the SpreadFEx campaing data. It was shown that tidal winds likely control the orientations of the AGWs that attain the highest altitudes and have the greatest effect. Moreover, the AGWs and tidal winds acting

together have an even greater potential impact on plasma instability growth rate and plasma bubble seeding.

As regards the impact of the DE3 tide on the R–T instability, we will adhere to the conclusions made by [Kil et al., 2015]. Their numerical calculations of the linear growth rate of the R–T instability using the SAMI2 model simulation results indicate that the effect of the daytime vertical **E×B** drift modulated by DE3 tide on the growth rate is negligible. In other words, it means that $P_{R\text{-}T}$ should be estimated as $P_{R\text{-}T}\sim$ const.

In frame of [Kudeki and Bhattacharyya, 1999] theory, it is possible to obtain the numerical estimation of the possible tide influence on seeding mechanism in the EPB generation. According to [Kudeki et al., 2007] the growth time of a single seeding perturbation is $\tau=1/\gamma \cong 2L/\mathbf{U}$ (s). Then the number (n_{seed}) of seeding perturbations generated per hour is $n_{seed} = 3600/\tau \cong 3600\mathbf{U}/2L$. Hence the occurrence probability of the seeding perturbations is $P_{seed} = n_{seed}/n \cong 3600\mathbf{U}/(2Ln)$, where n is the total number of the tests.

It is easy to obtain the ratio of their maximum/minimum: $(P_{max}/P_{min})_{seed} \cong \mathbf{U}_{max}/\mathbf{U}_{min}$, which is directly proportional to the ratio of the maximal/minimal zonal delta wind velocities modulated by DE3. It is known that the typical mean zonal wind velocity taken in equinox sunset hours (18–21 LT) at the bottom-side of the *F*-layer is ~100÷200 m/s [Liu et al., 2006; Fritts et al., 2008]. Taking into account that the typical zonal delta wind variations induced by DE3 cover the range of ±12 m/s (Figure 2a) [Häusler et al., 2007], we can obtain that the velocity varies at least from $\mathbf{U}_{min}$= 88 m/s up to $\mathbf{U}_{max}$= 112 m/s. It means that $(P_{max}/P_{min})_{seed} \cong 1.3$. Following the above-mentioned approach ($P_{R\text{-}T}\sim$ const), we can obtain the ratio of the maximal/minimal occurrence probability of the EPBs: $(P_{max}/P_{min})_{EPB} = (P_{max}/P_{min})_{seed} \cong 1.3$.

On the other hand, it is easy to estimate the same ratio of the P_{EPB} obtained in the actual observations. For this aim, let's take the values of the P_{EPB} derived by [Kil et al., 2015] from the ROCSAT data. These data are chosen intentionally, since they are the most close to the initial EPBs and shows the primary longitudinal EPB distributions (±6° MLAT, ~600 km) ([Kil et al., 2015], and the Figure 1 therein). According to these data taken in the equinox, the ratio may be estimated as $(P_{max}/P_{min})_{EPB} \cong 1.5$.

Therefore, the ratios derived from the actual observations and obtained by modeling approach are quite close (1.3 and 1.5). They are close in spite of the serious simplification ($P_{R\text{-}T}\sim$ const) used in the model estimation. So, it may be condsidered as a possible reply in the frequency of the EPB generation to the variability of the thermosphere zonal wind modulated by DE3 tide.

Hence, we should point that the thermosphere winds play a good part of the mediator of the troposphere tide influence, if the phase of the EPB production is under consideration. It seems the tide-induced thermosphere winds can "program" the longitudinal distributions of the future plasma bubbles in the primary moment of their generation, namely, during the seed perturbation development (P_{seed}). As a result, the longitudinal occurrence rate of the equatorial *F* region irregularities (P_{EFI}) (including the EPBs) is well managed by the tide-induced thermosphere winds ($P_{EFI} = P_{R\text{-}T}P_{seed}$).

(2) As it was mentioned early, the plasma bubbles (as charged depleted areas) are controlled by the magnetic field during their uplift and "stretching". During the uplifting, the plasma bubbles are also affected by the neutral winds, which may be modulated by the troposphere tide influence. The zonal winds are pointed as especially notable [Lühr et al., 2007]. Modulated zonal winds in combination with the geomagnetic field declination can enhance (reduce) the vertical field-aligned winds. In turn, the field-aligned winds lead to strengthening/weakening the diffusion spreading the charged particles along the magnetic tubes (fountain effect). The last one causes either the further plasma bubble "stretching" or its "locking". The plasma bubbles, maximally "stretching" under favorable condition, may be detected over low latitudes up to mid-latitudes. The electrons of the bulk plasma are affected by the similar way. It leads to strengthening/weakening of the fountain effect, causing Ne density growth/decrease at the crest of the EIA.

It is worthy to point the ionosphere altitudes, where the impact of the field-aligned winds may be the most effective. (Note that the plasma bubbles investigated in this study are observed at the topside ionosphere altitudes (~1100 km)). Since the neutral density decreases with an increase of altitude, the direct wind impact with the plasma bubble uplifting becomes increasingly weak. Namely, it is important in the region up to ~500 km, where ion-neutral collisions still play the primary role. In the region above ~500 km, however, the wind influence is rather weak, since ion-ion collisions become dominated. At last, it becomes absolutely negligible at the altitudes of the topside ionosphere/plasmasphere, where the neutral density is close to zero.

It would seem the "program" of the longitudinal EPB distributions, induced by zonal winds at the moment of the EPB generation, should be essentially corrected during this stage, since the new powerful factor as "magnetic field–field-aligned winds" is joined to the management. Now the plasma bubbles as

magnetized areas should basically repeat the behavior of the charged particles (e.g., electrons) but not the neutrals. It was expected that the longitudinal EPB variations appear to be the most similar to the EIA variations. However, the available results [Henderson et al., 2005; Li et al., 2008; Sidorova and Filippov, 2016] testify another. (The longitudinal EPB and EIA distributions have not perfect matches, $R \cong 0.37$.) Therefore, it is necessary to conclude that a previously set "program" is more successful in the competition with the mentioned factor.

Actually, the picture of the longitudinal EPB distributions is a response to the complex impact from several factors such as the geomagnetic field, **E×B** drift, winds etc. According to our results, the main transfer way of the troposphere influence is the direct impact of the thermosphere winds modulated by the DE3 tides. The global longitudinal EPB distribution controlled by the geomagnetic field may be essentially corrected (modulated) by such wind influence. The modulated winds can cause the development of the four-peak longitudinal distribution of the EPBs. The correlated position of these peaks, in turn, point that they are apparently induced by the troposphere DE3 tides.

5. Summary

The idea of the possible influence of the troposphere non-migrating tide (DE3) on the character of the longitudinal distributions of the equatorial plasma bubbles (EPBs) was under consideration. For this purpose, the detailed comparative analysis of the thermosphere and ionosphere characteristics having the typical four-peak wave structures was made. The longitudinal distributions of the topside ionosphere plasma bubbles were calculated by using the He^+ density depletion dataset based on the ISS-b satellite data acquired in 1978–1979 ($F_{10.7}$~200, ~1100 km). Also, we have used the equatorial mass density anomaly (EMA) and zonal neutral wind characteristics having the prominent "wave-like" longitudinal structures with wave number 4, which is uniquely associated with the influence of the troposphere DE3 tides [Häusler et al., 2007; Liu et al., 2009]. All the data used for comparison were obtained in the equinox seasons during high solar activity. The main our findings are the following.

(1) The characteristics of the thermosphere neutral components (~400 km) show the surprising resemblance with the longitudinal distributions of the EPBs (~1100 km).The correlation factor between

the EPB and EMA plots averaged over both hemispheres and both equinoxes appears as very significant (R≅0.8).

(2) Also, there is high correlation (R≅0.72) between the EPB variations taken in the Northern hemisphere (NH) during the vernal equinox and zonal delta wind variations.

(3) The numerical estimation of the $(P_{max}/P_{min})_{EPB}$ ratio based on [Kudeki and Bhattacharyya,1999] model was compared with the actual observations and showed good accordance (1.3 and 1.5).

The aforementioned results may be considered as evidence supporting the idea about the troposphere tide influence on the character of the longitudinal EPB distributions. Thermosphere zonal winds may be pointed as main transfer mediator of the troposphere DE3 tide energy. Namely, the eastward zonal winds affecting the EPBs during their production play a crucial role. It becomes possible, since they control the occurrence rate of the seed perturbations (starting condition of the EPB production).

References

Abdu, M.A. Outstanding problems in the equatorial ionosphere-thermosphere electrodynamics relevant to spread F. *J. Atmos. Terr. Phys.* **63**(9), 869-884, 2001.

Aggson, T.L., Maynard, N.C., Hanson, W.B., Saba, J.L. Electric field observations of equatorial bubbles. *J. Geophys. Res.* **97**, 2997-3009, 1992.

Basu, Su., Basu, S., Khan, B.K. Model of equatorial scintillation from in-situ measurements. *Radio. Sci.* **11**, 821-832, 1976.

Chen, A.J., Wolf, R.A. Effects on the plasmasphere of a time-varying convection electric field. *Planet. Space Sci.* **20**(4**)**, 483-505,1972.

Fang, T.W., Kil, H., Millward, G., Richmond, A.D., Liu, J.Y., Oh, S.J. Causal link of the wave-4 structures in plasma density and vertical plasma drift in the low-latitude ionosphere. *J. Geophys. Res.* **114**, A10315, doi: 10.1029/2009JA014460, 2009.

Forbes, J.M., Bruinsma, S.L., Zhang, X., Oberheide, J. Surface-exosphere coupling due to the thermal tides. *Geophys. Res. Lett.* **36**, L1581, doi: 10.1029/2009GL038748, 2009.

Fritts, D.C., Vadas, S.L., Riggin, D.M., Abdu, M.A., Batista, I.S. Takahashi, H., Medeiros, A., Kamalabadi, F., Liu, H.L., Fejer, B.G., Taylor, M.J., Gravity wave and tidal influences on equatorial spread F based on observations during the Spread *F* Experiment (SpreadFEx). *Ann. Geophysicae* **26**, 3235-3252, 2008.

Häusler, K., Lühr, H., Rentz, S., Köhler, W. A statistical analysis of longitudinal dependence of upper thermospheric zonal winds at dip equator latitudes derived from CHAMP. *J. Atmos. Sol. Terr. Phys.* **69**(12), 1419-1430, doi: 10.1016/j.jastp.2007.04.004, 2007.

Häusler, K., Lühr, H. Nonmigrating tidal signals in the upper thermospheric zonal wind at equatorial latitudes as observed by CHAMP. *Ann. Geophys.* **27**(7), 2643-2652, 2009.

Henderson, S.B., Swenson, C.M., Christensen, A.B., Paxton, L.J. Morphology of the equatorial anomaly and equatorial plasma bubbles using image subspace analysis of Global Ultraviolet Imager data. *J. Geophys. Res.* **110**, A11306, doi: 10.1029/2005JA011080, 2005.

Hysell, D.L., Kudeki, E. Collisional shear instability in the equatorial *F*-region ionosphere. *J. Geophys. Res.* **109**, A11301, doi: 10.1029/2004JA019636, 2004.

Immel, T.J., Sagawa, E., England, S.L., Henderson, S.B., Hagan, M.E., Mende, S.B., Frey, H.U., Swenson, C.M., Paxton, L.J. Control of equatorial ionospheric morphology by atmospheric tides. *Geophys. Res. Lett.* **33**, L15108, doi: 10.1029/2006GL026161, 2006.

Jin, H., Miyoshi, Y., Fujiwara, H., Shinagawa, H. Electrodynamics of the formation of ionospheric wave number 4 longitudinal structure. *J. Geophys. Res.* **113**, A09307, doi: 10.1029/2008JA013301, 2008.

Karpachev, A.T., Sidorova, L.N. Occurrence probability of the light ion trough and subtrough in He^+ density on season and local time. *Adv. Space Res.* **29**(6), 999-1008, 2002.

Karpachev, A.T., Sidorova, L.N. Distinction and classification of the troughs and subtroughs in He^+ density from ISS-b satellite data at 1000-1200 km altitudes. *J. Atmos. Sol. Terr. Phys.* **65**, 997-1006, 2003.

Kherani, E.A., Abdu, M.A., Fritts, D.C., De Paulo, E.R, 2011. Chapter 10. The Acoustic Gravity Wave Induced Disturbances in the Equatorial Ionosphere. In Aeronomy of the Earth's Atmosphere and Ionosphere. IAGA Special Sopron Book Series 2. Abdu, M.A., Pancheva, D. (Eds.) pp. 141–162 (Dordrecht-Heidelberg-London-New York: Springler Science+Business Media B), doi: 10.1007/978-94-007-0926-1.

Kil, H., Heelis, R.A., Paxton, L.J., Oh, S.J. Formation of a plasma depletion shell in the equatorial ionosphere, *J. Geophys. Res.* **114**, A11302, doi: 10.1029/2009JA014369, 2009.

Kil, H., Kwak, Y.-S., Lee, W.K., Krall, J., Huba, J.D., Su, S.J. Nonmigrating tidal signature in the distributions of equatorial plasma bubbles and prereversal enhancement. *J. Geophys. Res.* **120**(4), 3254-3262, doi: 10.1002/2014JA020908, 2015.

Kudeki, E., Bhattacharyya, S. Postsunset vortex in equatorial *F*-region plasma drifts and implications for bottomside spread F. *J. Geophys. Res.* **104**(12), 28163-28170, 1999.

Kudeki, E., Akgiray, A., Milla, M.A., Chau, J.L., Hysell, D.L. Equatorial spread-F initiation: post-sunset vortex, thermospheric winds, gravity waves. *J. Atmos. Sol. Terr. Phys.* **69**(17-18), 2416-2427, 2007.

Li, G., Ning, B., Liu, L., Ren, Z., Lei, J., Su, S.Y. The correlation of longitudinal/seasonal variations of evening pre-reversal drift and of plasma bubbles. *Ann. Geophys.* **25**, 2571-2578, doi: 10.5194/angeo-25-2571-2007, 2007.

Li, G., Ning, B., Liu, L., Zhao, B., Yue, X., Su, S.Y., Venkatraman, S. Correlative study of plasma bubbles, evening equatorial ionization anomaly, and equatorial prereversal **E×B** drifts at solar maximum. *Radio. Sci.* **43**, RS4005, doi: 10.1029/2007RS003760, 2008.

Liu, H., Lühr, H., Henize, V., Köhler, W. Global distribution of the thermospheric total mass density derived from CHAMP. *J. Geophys. Res.* **110**, A04301, doi: 10.1029/2004JA01741, 2005.

Liu, H., Lühr, H., Watanabe, S., Köhler, W., Henize, V., Visser, P. Zonal winds in the equatorial upper thermosphere: decomposing the solar flux, geomagnetic activity, and seasonal dependencies, *J. Geophys. Res.* **111**, A07307, doi: 10.1029/2005JA011415, 2006.

Liu, H., Watanabe, S. Seasonal variation of the longitudinal structure of the equatorial ionosphere: Does it reflect tidal influences from below? *J. Geophys. Res.* **113**, A08315, doi: 10.1029/2008JA013027, 2008.

Liu, H., Yamamoto, M., Lühr, H. Wave 4 pattern of the equatorial mass density anomaly: A thermospheric signature of tropical deep convection. *Geophys. Res. Lett.* **36**, L18104, doi: 10.1029/2009GL039865, 2009.

Lühr, H., Häusler, K., Stolle, C. Longitudinal variation of *F* region electron density and thermosphere zonal wind caused by atmospheric tides. *Geophys. Res. Lett.* **34**, L16102, doi: 10.1029/2007GL030639, 2007.

Maruyama, T., Matuura, N. Global distribution of occurrence probability of spread echoes based on ISS-b observation. *J. Radio Res. Lab.* **27**(124), 201-216, 1980.

Maruyama, T., Matuura, N. Longitudinal variability of annual changes in activity of equatorial spread *F* and plasma bubbles. *J. Geophys. Res.* **89**, A12, 10903-10912, 1984.

McClure, J.P., Singh, S., Bamgboye, D.K., Johnson, F.S., Kil, H. Occurrence of equatorial F region irregularities: Evidence for tropospheric seeding. *J. Geophys. Res*. **103**, 119-29, 1998.

Oberheide, J., Forbes, J., Häusler, K., Wu, Q., Bruinsma, S.L. Tropospheric tides from 80-400 km: propagation, inter-annual variability and solar cycle effects. *J. Geophys. Res.* **114**, D00105, doi: 10.1029/2009JD012388, 2009.

Oberheide, J., Forbes, J., Zhang, X., Bruinsma, S.L. Wave-driven variability in the ionosphere-thermosphere-mesosphere system from TIMED observations: What contributes to the "wave-4"? *J. Geophys. Res*. **116**, A01306, doi: 10.1029/2010JA015911, 2011.

Pedatella, N.M., Forbes, J.M., Maute, A., Richmond, A.D., Fang, T.-W., Larson, K.M., Millward, G. Longitudinal variations in the F region ionosphere and the topside ionosphere-plasmasphere: Observations and model simulations. *J. Geophys. Res.* **116**, A12309, doi: 10.1029/2011JA016600, 2011.

RRL, 1983. Summary Plots of Ionospheric Parameters obtained from Ionosphere Sounding Satellite-b. Radio Research Laboratories Ministry of Posts and Telecommunications, Tokyo 1-3.

RRL, 1985. Summary Plots of Ionospheric Parameters obtained from Ionosphere Sounding Satellite-b. Radio Research Laboratories Ministry of Posts and Telecommunications, Tokyo Special Report 4.

Sidorova, L.N. He^+ density topside modeling based on ISS-b satellite data. *Adv. Space Res.* **33**, 850-854, 2004.

Sidorova, L.N. Plasma bubble phenomenon in the topside ionosphere. *Adv. Space Res.* Special issue (COSPAR) **39**(8), 1284-1291, doi: 10.1016/j.asr.2007.03.067, 2007.

Sidorova, L.N. Topside plasma bubbles, seen as He^+ density depletions. In *Proceedings of the Conference on Fundamental Space Research*, ISTI BAS, Sunny Beach, Bulgaria, 238-241, 2008.

Sidorova, L.N., Filippov, S.V. Topside ionosphere He^+ density depletions: seasonal/longitudinal occurrence probability. *J. Atmos. Sol. Terr. Phys.* **86**, 83-91, doi: 10.1016/j.jastp.2012.06.013, 2012.

Sidorova, L.N., Filippov, S.V. Plasma bubbles in the topside ionosphere: estimations of the survival possibilities. *J. Atmos. Sol. Terr. Phys.* **119**, 35-41, doi: 10.1016/j.jastp.2014.06.013, 2014.

Sidorova, L.N., Filippov, S.V. Longitudinal statistics of plasma bubbles: Possible tropospheric influence. *Geomagn. Aeron.* **56**(4), 482-492, doi: 10.1134/S0016793216040198, 2016.

Singh, S.F., Johnson, F.S., Power, R.A. Gravity wave seeding of equatorial plasma bubbles. *J. Geophys. Res.* **102**, 7399-7410, 1997.

Su, S.Y., Liu, C.H., Ho, H.H., Chao, C.K. Distribution characteristics of topside ionospheric density irregularities: Equatorial versus midlatitude regions. *J. Geophys. Res.* **111**, A06305, doi: 10.1029/2005JA011330, 2006.

Talaat, E.R., Lieberman, R.S. Direct observations of nonmigrating diurnal tides in the equatorial thermosphere. *Geophys. Res. Lett*. **37**, L04803, doi: 10.1029/2009GL041845, 2010.

Tsunoda, R. T. On seeding equatorial spread *F* during solstices. *Geophys. Res. Lett.* **37**(5), 5-8, doi: 10.1029/2010GL042576, 2010.

Yizengaw, E. Global longitudinal dependence observation of the neutral wind and ionospheric density distribution. *Int. J. Geophys.* **2012**, ID 342581, doi: 10.1155/2012/342581, 2012.

Watanabe, S., Oya, H. Occurrence characteristics of low latitude ionospheric irregularities observed by impedance probe on board the Hinotori satellite. J. *Geomagn. Geoelectr.* **38**, 125-149, 1986.

Watanabe, S., Oyama, K.I. Effects of neutral wind on the electron temperature at a height of 600 km in the low latitude region. *Ann. Geophys.* **14**, 290-296, 1996.

Woodman, R.F., La Hoz, C. Radar observations of *F*-region equatorial irregularities. *J. Geophys. Res.* **81**, 5447-5466, 1976.